Hindawi
Mathematical Problems in Engineering
Volume 2018, Article ID 3612697, 14 pages
https://doi.org/10.1155/2018/3612697

Research Article

Qualitative Analysis of the Evolution Behaviors of Irradiation-Induced Point Defects

Hao Huang, Shurong Ding, and Yongzhong Huo

Institute of Mechanics and Computational Engineering, Department of Aeronautics and Astronautics, Fudan University, Shanghai 200433, China

Correspondence should be addressed to Yongzhong Huo; yzhuo_cd@hotmail.com

Received 15 May 2018; Accepted 5 June 2018; Published 28 June 2018

Academic Editor: Guang-Yong Sun

Point defects created by the collisions of high-energy particles and their subsequent evolutions form the foundation for all observed irradiation effects. Qualitative analysis is performed for the local and global behaviors of the planar system of nonlinear ordinary differential equations for the point defects balance model. The results indicated that the evolution behavior for the in-pile process is qualitatively very similar to the more simple annealing process, but very different from the degenerated systems that possess analytical solutions. However, quantitatively, irradiations in the in-pile process will shift the stable node away from the defect free state and change the local behaviors. A too strong irradiation may result in a nonphysical stable node and produce amorphous states, thus making the model inadequate.

1. Introduction

In irradiate environments, solid atoms can be displaced from their lattice sites and become interstitial atoms by the collisions of high-energy particles [1, 2]. The generated point defects (vacancies and interstitials, known as the Frenkel pairs) and their subsequent evolutions form the foundation for all observed irradiation effects on the physical and mechanical properties of materials. Notably irradiation-induced mechanical degradations include the volumetric swelling, creep instabilities, increase in hardness, loss of ductility, and also cracking [1, 3]. Thus, a proper understanding of their evolution behavior is at the central of the radiation damage.

Experimental and theoretical studies have shown that the point defects evolution is mainly governed by three different mechanisms, the production rate, the recombination rate, and the annihilation rate [4–12]. The rate of point defects production depends on the irradiation conditions and the material types. The irradiation generated pairs of vacancies and interstitials can get lost due to their recombination and the recombination rate is mainly determined by their diffusions. They can also be lost to sinks such as voids, dislocation loops, and grain boundaries. The annihilation rates depend on their diffusions and the sink concentrations and strengths [1, 13].

By using the defect reaction rate theory, a planar system of nonlinear ordinary differential equations (ODEs), named the point defect balance equations (PDBEs), has been proposed by Lomer [9] for the evolution of the spatially averaged point defects concentrations ($c_v(t)$, $c_i(t)$) for materials under irradiations. The system is quadratic in c_v and c_i with a constant production rate and four additional material constants representing the recombination and the annihilation mechanisms, respectively. The system has been used widely as a standard model for the evolution behavior of the irradiation-induced point defects. Analytical solutions were obtained for several degenerated systems in which some mechanisms are neglected and the corresponding material constants are assumed null. Although such analytical solutions are very helpful, they cannot be directly extrapolated to the original nondegenerated (UD) system. Many numerical solutions have been obtained and can provide useful information [5, 14, 15]. However, a proper understanding of the solution behaviors of PDBEs and the effect of the three different mechanisms are still lacking.

In this paper, the qualitative (geometrical) method of ODEs [16, 17] is utilized to study the solution behavior of

PDBEs. After introducing the planar system, the singular points are obtained and their local behaviors are discussed in the next section. In Section 3, the global behavior is analyzed in the phase plane. Considering the behavior at infinity, the global phase portraits are also obtained on the Poincaré disk. Possible physical admissible conditions are discussed in Section 4. A numerical example is also presented before the conclusion to illustrate the difference between degenerated and nondegenerated systems.

2. Balance Equations and Local Behaviors Near Singular Points

2.1. Point Defects Balance Equations (PDBEs). The Frenkel defects are generated by collisions cascade and can be lost through either recombination or reaction with defect sinks. So the defect concentration of vacancy and interstitial is the balance between (1) local production rate, (2) reaction with other species, and (3) diffusion into or out of the local volume. The balance equations of the irradiation-induced point defects are [1, 5]

$$\begin{aligned} \frac{dc_v}{dt} &= K_0 - K_{iv}c_v c_i - K_{vs}c_s c_v \\ \frac{dc_i}{dt} &= K_0 - K_{iv}c_v c_i - K_{is}c_s c_i \end{aligned} \tag{1}$$

where

(1) $c_{v,i}$ is the atom fraction of vacancy/interstitial, or vacancy/interstitial concentration;

(2) K_0 is the defect production rate by radiation;

(3) K_{iv} is the recombination rate coefficient of vacancy and interstitial;

(4) $K_{v,is}$ is the vacancy/interstitial-sink reaction rate coefficients;

(5) c_s is the sink density.

The parameters K_0, K_{iv}, $K_{v,is}$, and c_s in (1) are nonnegative constants. And we have $K_{is} > K_{vs}$ for sinks absorb interstitials at faster rates than vacancies.

Let $x = c_v$ and $y = c_i$; if $K_{iv} > 0$, system (1) becomes

$$\begin{aligned} \frac{dx}{dt} &= -xy - ax + c = \widetilde{P}(x, y) \\ \frac{dy}{dt} &= -xy - by + c = \widetilde{Q}(x, y) \end{aligned} \tag{2}$$

where

$$\begin{aligned} a &= \frac{K_{vs}c_s}{K_{iv}}, \\ b &= \frac{K_{is}c_s}{K_{iv}}, \\ c &= \frac{K_0}{K_{iv}}, \\ \widetilde{t} &= K_{iv}t \end{aligned} \tag{3}$$

For simplicity, the superscript of $\widetilde{t}$, $\widetilde{P}$, and $\widetilde{Q}$ in the following contents will be neglected.

We will discuss the following two different processes separately.

(1) Annealing: $K_0 = 0$, i.e., $c = 0$, no point defect source. Thus, the defects could only annihilate by recombination or in sinks.

(2) In-pile irradiation: $K_0 > 0$, i.e., $c > 0$. Thus, the point defects are generated as the material is exposed in irradiate environments.

2.2. Singular Points and Local Behaviors

2.2.1. Annealing: $c = 0$. First, we will discuss the properties of the singular points and the local behaviors near them during annealing process. In system (2), by letting $P(x, y) = Q(x, y) = 0$, we can get the singular points.

Theorem 1. *If $a, b > 0$ and $c = 0$, system (2) has two singular points*

$$\begin{aligned} (x_1, y_1) &= (0, 0), \\ (x_2, y_2) &= (-b, -a) \end{aligned} \tag{4}$$

The local behaviors near the two singular points are easily obtained as follows.

Theorem 2. *If $a, b > 0$ and $c = 0$, the singular point $(x_1, y_1) = (0, 0)$ (4) is a stable node. And the local behaviors of system (2) near the stable node are*

$$\begin{pmatrix} x(t) \\ y(t) \end{pmatrix} = \begin{pmatrix} \exp(-at) & 0 \\ 0 & \exp(-bt) \end{pmatrix} \begin{pmatrix} x_0 \\ y_0 \end{pmatrix} \tag{5}$$

and the trajectories satisfy

$$x^{-b}y^{a} = Const. \tag{6}$$

Proof. At $(x_1, y_1) = (0, 0)$, the Jacobi matrix of system (2) is

$$\mathbf{J}(x_1, y_1) = -\begin{pmatrix} a & 0 \\ 0 & b \end{pmatrix} \tag{7}$$

Both eigenvalues of $\mathbf{J}(x_1, y_1)$ are negative real number and $(x_1, y_1) = (0, 0)$ is a stable node. The local behaviors could be easily obtained. □

The phase portraits are shown in Figure 1(a); the decrease of y is much faster than x, because sinks absorb interstitials at faster rates than vacancies, i.e., $b > a > 0$. Besides, as shown in Figure 1(b), x/x_0 versus y/y_0 under the different value of $\delta = a/b$, it is easy to find that the smaller δ leads to the steeper curve for the faster decrease of y.

Theorem 3. *If $a, b > 0$ and $c = 0$, the singular point $(x_2, y_2) = (-b, -a)$ (4) is a saddle point. And the local behaviors of system (2) near the saddle point are*

$$\begin{pmatrix} x(t) - x_2 \\ y(t) - y_2 \end{pmatrix}$$

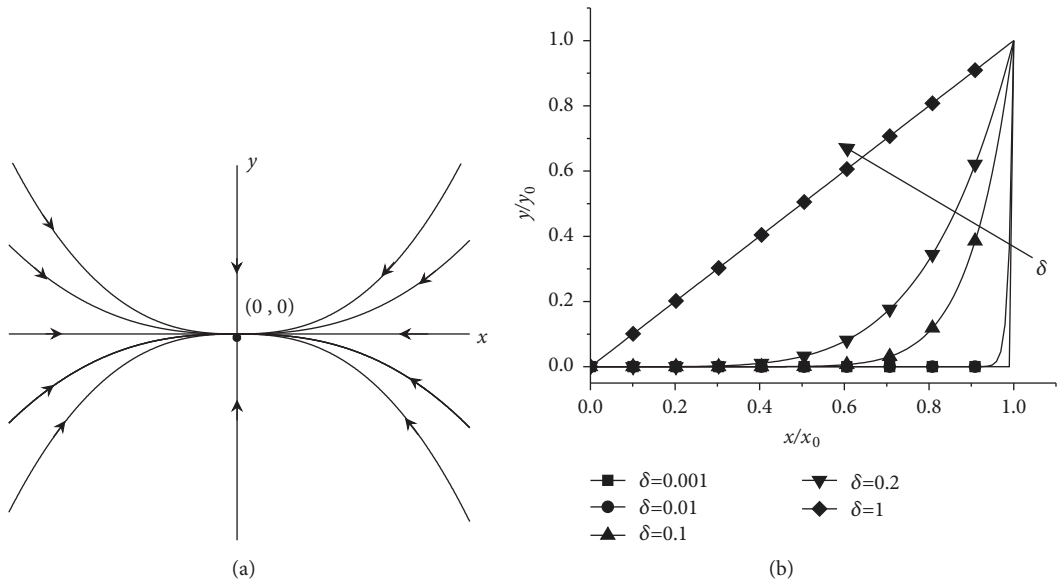

FIGURE 1: (a) Phase portraits near stable node $(0, 0)$ and (b) y/y_0 versus x/x_0 under different $\delta = a/b$ if $c = 0$.

$$= \mathbf{P}_2 \begin{pmatrix} \exp\left(\sqrt{ab}t\right) & 0 \\ 0 & \exp\left(-\sqrt{ab}t\right) \end{pmatrix} \mathbf{P}_2^{-1} \begin{pmatrix} x_0 - x_2 \\ y_0 - y_2 \end{pmatrix} \tag{8}$$

where

$$\mathbf{P}_2 = \begin{pmatrix} 1 & -1 \\ \sqrt{\frac{a}{b}} & \sqrt{\frac{a}{b}} \end{pmatrix} \tag{9}$$

and the trajectories satisfy

$$a(x+b)^2 - b(y+a)^2 = Const. \tag{10}$$

Proof. At $(x_2, y_2) = (-b, -a)$, the Jacobi matrix of system (2) is

$$\mathbf{J}(x_1, y_1) = \begin{pmatrix} 0 & b \\ a & 0 \end{pmatrix} \tag{11}$$

The eigenvalues of $\mathbf{J}(x_2, y_2)$ are $\lambda_{1,2} = \pm\sqrt{ab}$: one is a positive and the other is a negative real number, so (x_2, y_2) is a saddle point. And the local behaviors could be easily obtained. □

The phase portraits are shown in Figure 2(a). For the same constant, the trajectories of different $\delta = a/b$ in the first quadrant are shown in Figure 2(b). It could be found that the larger δ leads to the larger slope of the asymptotic line and the larger y for the same x.

2.2.2. In-Pile Irradiation: $c > 0$. After introducing the source term, the singular points become as follows.

Theorem 4. *If $a, b > 0$ and $c > 0$, system (2) has two singular points*

$$x_{1,2} = -\frac{b}{2}\left(1 \mp \sqrt{1 + \frac{4c}{ab}}\right),$$
$$y_{1,2} = -\frac{a}{2}\left(1 \mp \sqrt{1 + \frac{4c}{ab}}\right) \tag{12}$$

Compared with the annealing process, after introducing the source term, we know that the amount of the singular point has not been changed. But the position of the stable node (x_1, y_1) is shifted to the first quadrant. And (x_2, y_2) is still in the third quadrant. The local behaviors near the singular points are as follows.

Theorem 5. *If $a, b > 0$ and $c > 0$, the singular point (x_1, y_1) (12) of system (2) is a stable node in the first quadrant, and the local behaviors near the stable node are*

$$\begin{pmatrix} x(t) - x_1 \\ y(t) - y_1 \end{pmatrix} = \mathbf{P}_1 \begin{pmatrix} \exp\left(\lambda_1^+ t\right) & 0 \\ 0 & \exp\left(\lambda_1^- t\right) \end{pmatrix} \mathbf{P}_1^{-1} \begin{pmatrix} x_0 - x_1 \\ y_0 - y_1 \end{pmatrix} \tag{13}$$

where $\mathbf{P}_1 = (\mathbf{v}_1^+, \mathbf{v}_1^-)$ and the eigenvalues $\lambda_1^\pm$ and $\mathbf{v}_1^\pm$ eigenvectors of the Jacobi matrix are

$$\lambda_1^\pm = -\frac{a+b}{4}\left(1 + \sqrt{1 + \frac{4c}{ab}}\right) \pm \frac{\sqrt{\Delta_1}}{2} \tag{14}$$

$$\mathbf{v}_1^\pm == \frac{1}{\sqrt{1 + \left(\varphi_1^\pm\right)^2}} \begin{pmatrix} 1 \\ \varphi_1^\pm \end{pmatrix} \tag{15}$$

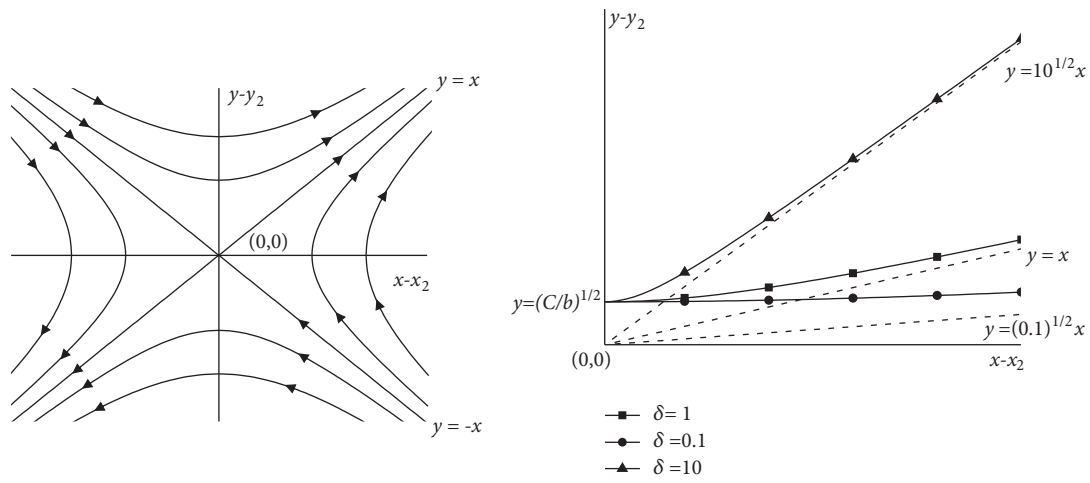

FIGURE 2: (a) Phase portraits near saddle point (x_2, y_2) and (b) local trajectories under different $\delta = a/b$ if $c = 0$.

where

$$\Delta_1 = \frac{1}{4}\left[(a+b)^2\left(1+\sqrt{1+\frac{4c}{ab}}\right)^2 - 16ab\sqrt{1+\frac{4c}{ab}}\right] \quad (16)$$

$$\varphi_1^{\pm} = \frac{(b-a)\left(\sqrt{1+4c/ab}+1\right) \mp 2\sqrt{\Delta_1}}{2b\left(\sqrt{1+4c/ab}-1\right)} \quad (17)$$

Proof. At (x_1, y_1) (12), the Jacobi matrix of system (2) is

$$\mathbf{J}(x_1, y_1) = \begin{pmatrix} -\frac{a}{2}\left(1+\sqrt{1+\frac{4c}{ab}}\right) & \frac{b}{2}\left(1-\sqrt{1+\frac{4c}{ab}}\right) \\ \frac{a}{2}\left(1-\sqrt{1+\frac{4c}{ab}}\right) & -\frac{b}{2}\left(1+\sqrt{1+\frac{4c}{ab}}\right) \end{pmatrix} \quad (18)$$

The trace and the determinant of $\mathbf{J}(x_1, y_1)$ are

$$T_1 = -\frac{a+b}{2}\left(1+\sqrt{1+\frac{4c}{ab}}\right) \quad (19)$$

$$J_1 = ab\sqrt{1+\frac{4c}{ab}} \quad (20)$$

So we have $T_1 < 0, J_1 > 0$. And it is easy to find that $\Delta_1 \geq 0$ for $(a+b)^2 \geq 4ab$ and $(1+\sqrt{1+4c/ab})^2 \geq 4\sqrt{1+4c/ab}$. The eigenvalues of Jacobi matrix are

$$\lambda_1^{\pm} = \frac{T_1 \pm \sqrt{\Delta_1}}{2} \quad (21)$$

By definition, we have $T_1 \pm \sqrt{\Delta_1} < 0$ and $\lambda_1^{\pm} < 0$. So the singular point (x_1, y_1) is a stable node. □

Theorem 6. *If $a, b > 0$ and $c > 0$, the singular point (x_2, y_2) (12) of system (2) is a saddle point in the third quadrant. And the local behaviors near the saddle point are*

$$\begin{pmatrix} x(t) - x_2 \\ y(t) - y_2 \end{pmatrix} = \mathbf{P}_2' \begin{pmatrix} \exp(\lambda_2^+ t) & 0 \\ 0 & \exp(\lambda_2^- t) \end{pmatrix} \mathbf{P}_2'^{-1} \begin{pmatrix} x_0 - x_2 \\ y_0 - y_2 \end{pmatrix} \quad (22)$$

where $\mathbf{P}_2' = (\mathbf{v}_2^+, \mathbf{v}_2^-)$ and the eigenvalues $\lambda_2^{\pm}$ and $\mathbf{v}_2^{\pm}$ eigenvectors of the Jacobi matrix are

$$\lambda_2^{\pm} = -\frac{a+b}{4}\left(1-\sqrt{1+\frac{4c}{ab}}\right) \pm \frac{\sqrt{\Delta_2}}{2} \quad (23)$$

$$\mathbf{v}_2^{\pm} == \frac{1}{\sqrt{1+(\varphi_2^{\pm})^2}}\begin{pmatrix} 1 \\ \varphi_2^{\pm} \end{pmatrix} \quad (24)$$

where

$$\Delta_2 = \frac{1}{4}\left[(a+b)^2\left(1-\sqrt{1+\frac{4c}{ab}}\right)^2 + 16ab\sqrt{1+\frac{4c}{ab}}\right] \quad (25)$$

$$\varphi_2^{\pm} = \frac{(b-a)\left(\sqrt{1+4c/ab}-1\right) \pm 2\sqrt{\Delta_2}}{2b\left(\sqrt{1+4c/ab}+1\right)} \quad (26)$$

Proof. Similarly, at (x_1, y_1) (12), the eigenvalues of the Jacobi matrix are

$$\lambda_2^{\pm} = \frac{T_2 \pm \sqrt{\Delta_2}}{2} \quad (27)$$

where

$$T_2 = -\frac{a+b}{2}\left(1-\sqrt{1+\frac{4c}{ab}}\right) \quad (28)$$

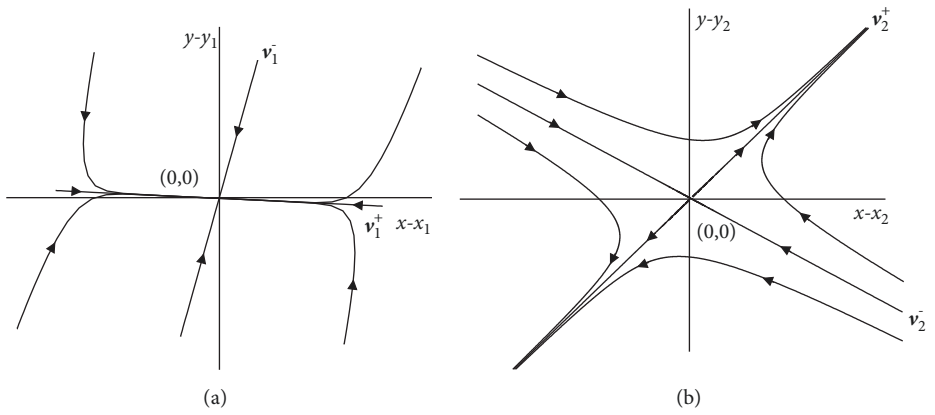

Figure 3: Phase portraits near (a) stable node (x_1, y_1) and (b) saddle point (x_2, y_2) if $c > 0$.

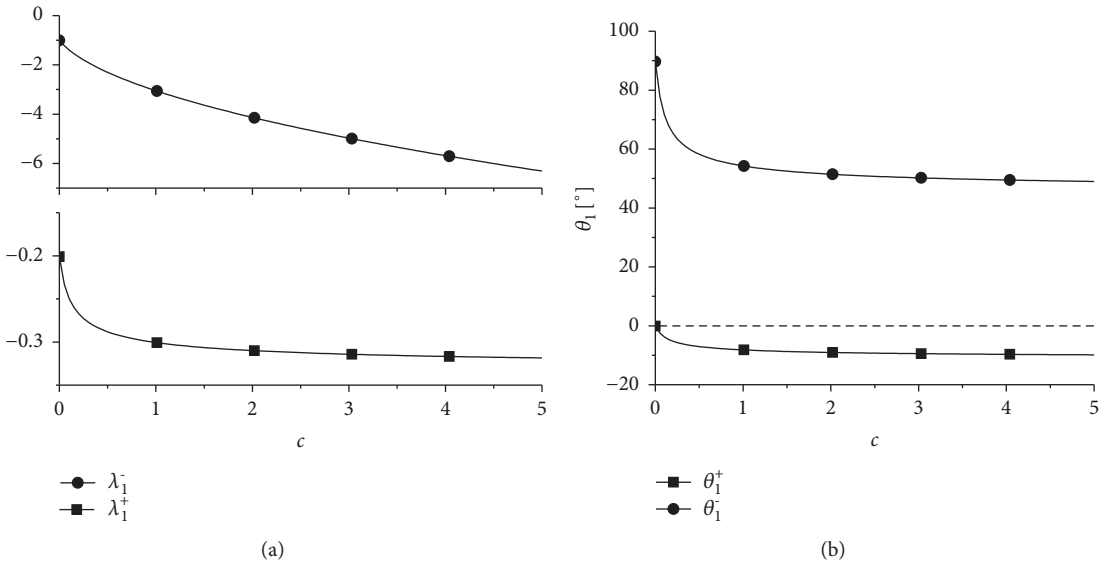

Figure 4: (a) Eigenvalue $\lambda_1^{\pm}$ and (b) angle between eigenvector $\mathbf{v}_1^{\pm}$ and x axis $\theta_1^{\pm}$ versus c.

It is easy to find that T_2 and $\Delta_2 > 0$. Besides, $T_2 + \sqrt{\Delta_2} > 0$, $T_2 - \sqrt{\Delta_2} < 0$, and $\lambda_2^+ > 0 > \lambda_2^-$. So the singular point (x_2, y_2) is a saddle point. □

As shown in Figure 3, in the in-pile process, x or y will no longer approach or deviate the singular points along the coordinate axis. Because the eigenvectors are different from the annealing process, also, y decreases faster than x for sinks absorb interstitials at faster rates than vacancies. The trajectories tend to the eigenvector $\mathbf{v}_1^+$ near the stable node (x_1, y_1). The trajectories tend to $\mathbf{v}_2^+$ near the saddle point (x_2, y_2).

Next, we analyze the effects of defects production rate on the eigenvalues and eigenvectors. As shown in Figure 4, with the increase of the defects production rate c, λ_1^+ will always decrease. But λ_1^- will decrease first and then remain almost constant for c large enough. Define $\theta_1^{\pm} = \arctan(\varphi_1^{\pm})$ as the angle between $\mathbf{v}_1^{\pm}$ and x axis. We found that, with the increase of c, $\theta_1^{\pm}$ will decrease first and then remain almost constant for c large enough. The effects of c on $\lambda_2^{\pm}$ and $\varphi_2^{\pm}$ are similar, as shown in Figure 5.

2.3. Some Degenerated Systems. Under some extreme conditions, one or more effects in system (2) are small enough and can be neglected. We get some degenerated systems.

(1) Sink-Free Limit (SFL): $c_s = 0$, i.e., $a = b = 0$, negligible defects-sink reactions. Thus, the point defects can only annihilate due to recombination and system (2) becomes symmetric.

(2) Low Temperature Limit (LTL): $K_{vs} \approx 0$, i.e., $a = 0$, negligible vacancy-sink reaction. Thus, the vacancies can only annihilate due to recombination.

(3) High Temperature Limit (HTL): $K_{iv} \approx 0$. The defect annihilation rate at the sinks keeps the concentration of interstitial low, such that recombination does not contribute much.

Compared to UD, the singular points degenerate to singular lines in SFL.

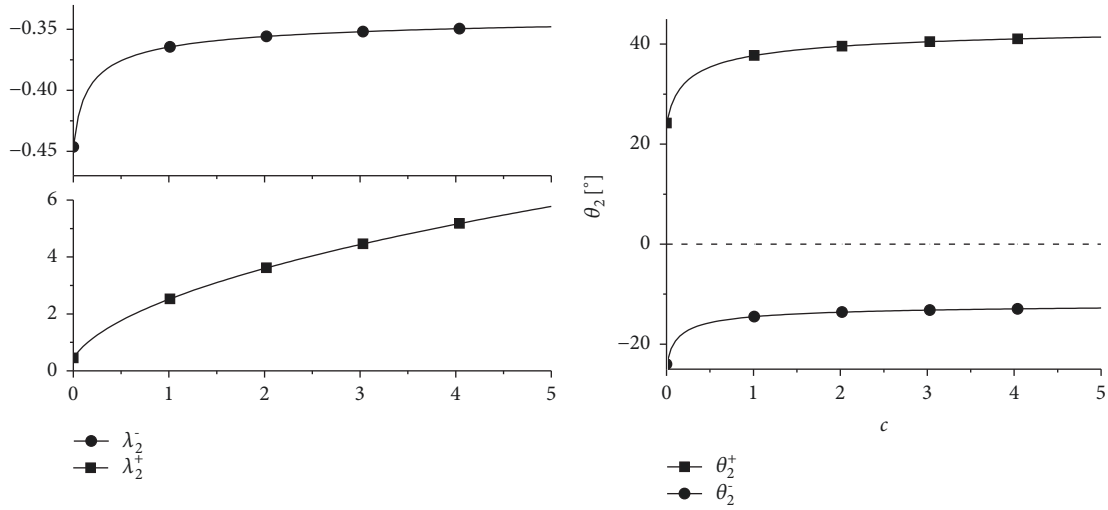

FIGURE 5: (a) Eigenvalue $\lambda_2^{\pm}$ and (b) angle between eigenvector $\mathbf{v}_2^{\pm}$ and x axis $\theta_2^{\pm}$ versus c.

Theorem 7. *(i) If $a = b = c = 0$, the singular lines of system (2) are $x = 0$ and $y = 0$; ii) if $a = b = 0$ and $c > 0$, the singular lines of system (2) are $xy = c$.*

Theorem 8. *If $a = b = 0$, the singular lines of system (2) are asymptotically stable only if $x, y > 0$ and unstable if $x, y < 0$. $(x, y) = (0, 0)$ is a saddle-node.*

Corollary 9. *If $a = b = 0$, the trajectories of system (2) satisfy $y = x - \Delta c_0$, where $\Delta c_0 = x_0 - y_0$. And the solutions are as follows:*

(i) if $c = 0$ and $\Delta c_0 = x_0 - y_0$,

$$y(t) = x(t) = \frac{x_0}{1 + x_0 t}, \tag{29}$$

(ii) if $c = 0$ and $\Delta c_0 \neq x_0 - y_0$,

$$\begin{aligned} x(t) &= \frac{1}{2}\left(x_0 - y_0 - \sqrt{\Delta_s}\right) \\ &\quad + \sqrt{\Delta_s}\left(1 - \frac{x_0 + y_0 - \sqrt{\Delta_s}}{x_0 + y_0 + \sqrt{\Delta_s}} \exp\left(-\sqrt{\Delta_s} t\right)\right)^{-1} \\ y(t) &= x(t) + \Delta c_0, \end{aligned} \tag{30}$$

where $\Delta_s = \Delta c_0^2$,

(iii) if $c > 0$, the solutions have the same form as (30), but $\Delta_s = \Delta c_0^2 + 4c$.

For SFL system, the balance equations (2) are symmetric. Lines $P = 0$ and $Q = 0$ are the same, which is $xy = c$. The stable node (x_1, y_1) degrades to asymptotic stable part of the singular line $xy = c (x > 0)$, and the saddle-node (x_2, y_2) degrades to unstable part of $xy = c (x < 0)$. The local behaviors near the singular lines are shown in Figure 6.

If only vacancy-sink reaction is negligible, the singular line is quite different compared to the previous system.

Theorem 10. *If $a = 0$, $b > 0$, the singular line of system (2) is $y = 0$ if $c = 0$. System (2) does not have any singular point if $c > 0$.*

Corollary 11. *If $a = 0$, $b > 0$, and $c = 0$, the singular line $y = 0$ is asymptotically stable only if $x > -b$ and unstable if $x < -b$. And the trajectories satisfy*

$$y - x + b \ln |x| = Const. \tag{31}$$

For LTL system, for vacancy-sink reactions are too small and negligible, we have $a = 0$ and $b > 0$. During annealing process, the stable node (x_1, y_1) degrades to asymptotic stable part of the singular line $y = 0 (x > -b)$, and the saddle-node (x_2, y_2) degrades to unstable part $y = 0 (x < -b)$. In in-pile process, the stable node and the saddle-node could not be found. The local behaviors near the singular line are shown in Figure 7.

At high temperatures, the recombination does not contribute much and could be neglected. System (1) becomes a linear system, and we can easily get the following analytical solutions.

Theorem 12. *If $K_{iv} = 0$, and*

(i) $K_{v,is} c_s > 0$, the only stable node is $(x^{\infty}, y^{\infty}) = (K_0/K_{vs} c_s, K_0/K_{is} c_s)$ and the solutions are

$$\begin{aligned} x(t) &= x^{\infty} + \left(x_0 - x^{\infty}\right) \exp\left(-K_{vs} c_s t\right) \\ y(t) &= y^{\infty} + \left(y_0 - y^{\infty}\right) \exp\left(-K_{is} c_s t\right); \end{aligned} \tag{32}$$

the trajectories satisfy

$$\left(x - x^{\infty}\right)^{-b} \left(y - y^{\infty}\right)^{a} = Const; \tag{33}$$

(ii) $c_s = 0$, there is no singular point; the solutions and the trajectories are

$$x = x_0 + K_0 t,$$

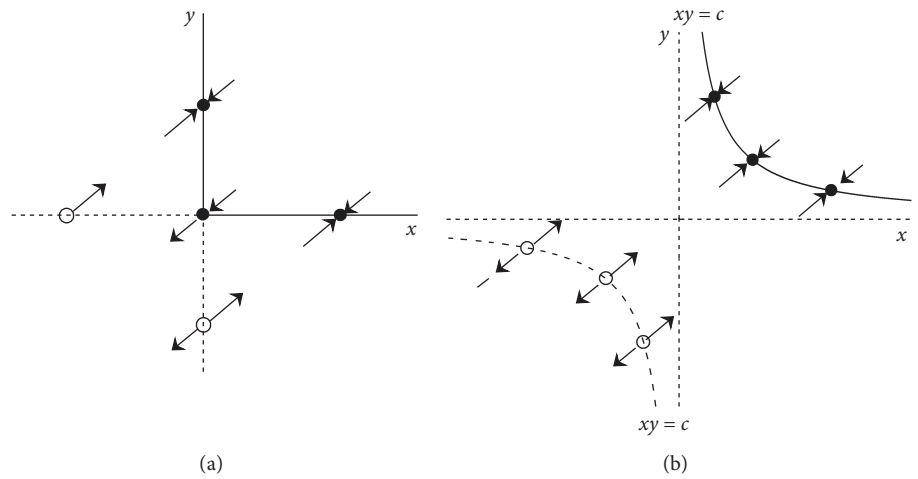

Figure 6: Phase portraits near singular lines of system (2) if (a) $a = b = c = 0$ and (b) $a = b = 0, c > 0$.

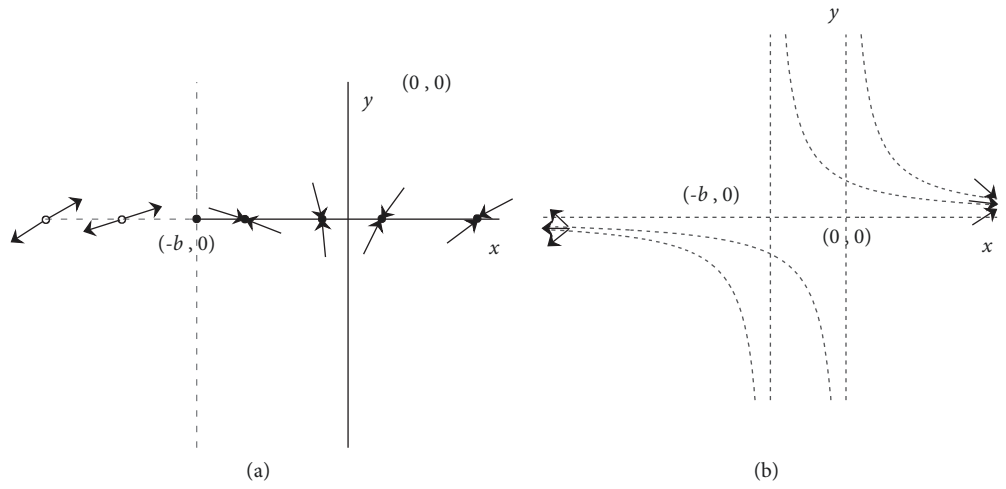

Figure 7: Phase portraits near singular lines or points of system (2) if (a) $a = 0, b > 0, c = 0$ and (b) $a = 0, b > 0, c > 0$.

$$y = y_0 + K_0 t,$$
$$x - y = Const; \tag{34}$$

(iii) $K_{vs} = 0$, $K_{is} > 0$, *and* $c_s = 0$, *the singular line is* $y = 0$ *if* $K_0 = 0$ *and there is no singular point if* $K_0 > 0$. *The solutions are*

$$x(t) = x_0 + K_0 t$$
$$y(t) = y^{\infty} + \left(y_0 - y^{\infty}\right) \exp\left(-K_{is} c_s t\right) \tag{35}$$

3. Global Behaviors and Phase Plane Portraits

3.1. Nonexistence of Closed Trajectories. Before we discuss the global behaviors of system (2), we should prove the nonexistence of closed trajectory first.

Lemma 13. *There is no closed trajectory of system (2) that can cross the x or y axis.*

Proof. At x axis, $y \equiv 0$, we have $\dot{y} = c \geq 0$ in system (2). And y always increases if $c > 0$ and unchanged if $c = 0$.

Assuming there exists a closed trajectory crossing x axis, y must decrease at one point and increase at another point, and $\dot{y} = c \geq 0$ is no longer satisfied, such that there is no closed trajectory crossing x axis. Similarly, there is no closed trajectory crossing y axis. □

Corollary 14. *The closed trajectory of system (2) must be completely inside one of the quadrants of* $x - y$ *plane; i.e.,*

$$\Omega_1 = \{x > 0, y > 0\},$$
$$\Omega_2 = \{x < 0, y > 0\}$$
$$\Omega_3 = \{x < 0, y < 0\},$$
$$\Omega_4 = \{x > 0, y < 0\} \tag{36}$$

Theorem 15. *If* $c = 0$ *and* $a, b > 0$, *system (2) has no closed trajectory.*

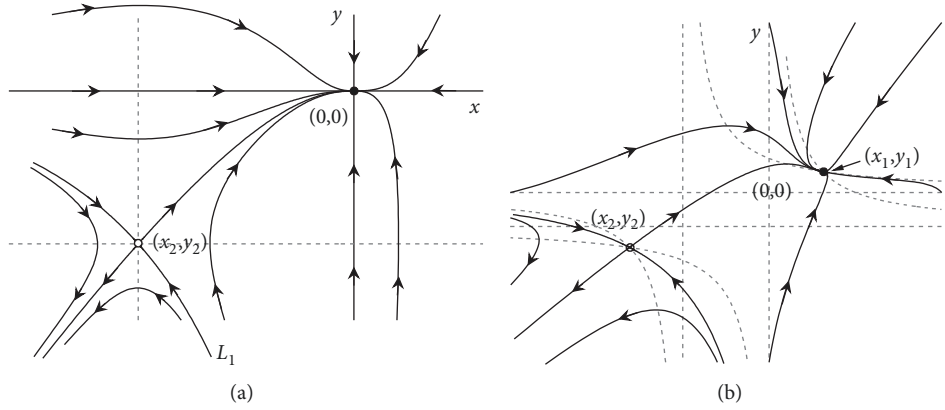

Figure 8: Phase plane portraits of system (2) with $a, b > 0$ and (a) $c = 0$ and (b) $c > 0$.

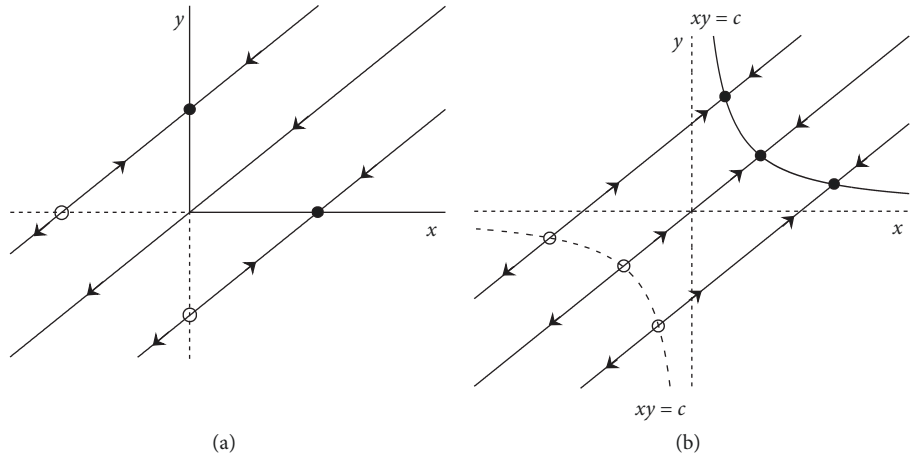

Figure 9: Phase plane portraits of system (2) with $a = b = 0$ and (a) $c = 0$ and (b) $c > 0$.

Proof. If $c = 0$, the stable node is $(x_1, y_1) = (0, 0)$ and the saddle point is $(x_2, y_2) = (-b, -a) \in \Omega_3$. By Lemma 13, the closed trajectory could only exist inside the quadrant which contains singular point. Besides, the singular point in Ω_3 is a saddle point, so system (2) has no closed trajectory. □

Theorem 16. *If $c > 0$ and $a, b > 0$, system (2) has no closed trajectory.*

Proof. If $c > 0$, the stable node $(x_1, y_1) \in \Omega_1$ and the saddle point $(x_2, y_2) \in \Omega_3$. There is no closed trajectory in Ω_2, Ω_3, and Ω_4. Inside Ω_1, we have

$$\frac{\partial P}{\partial x} + \frac{\partial Q}{\partial y} = -(a + b + x + y) < 0 \tag{37}$$

So there is no closed trajectory in Ω_1. □

3.2. Phase Plane Portraits. If $a, b > 0$, the phase plane portraits of system (2) are shown in Figure 8. For annealing ($c = 0$) and in-pile ($c > 0$) process, the portraits are qualitative similar. Only if x_0 and y_0 are small enough (lower than the asymptotic line L_1), the trajectories will approach to negative infinity. Others will approach to the stable node (x_1, y_1) (12).

The phase plane portraits of SFL system are shown in Figure 9. During annealing process, as shown in Figure 9(a), in the first quadrant, if $x_0 > y_0$, the trajectories evolve to x axis and only vacancies are left at last. Otherwise if $x_0 < y_0$, only interstitials are left at last. Only if $x_0 = y_0$, the system becomes defect free in the end. During the in-pile process, for the introducing of source term, both defects always exist at last.

The phase plane portraits of LTL system are shown in Figure 10. During annealing process, in the first quadrant, if $x_0 > 0$, the trajectories evolve to axis and only vacancies are left at last. And if $x_0 = 0$, the trajectories will evolve to origin, as shown in Figure 10(a). But during in-pile process, for there is no singular point, we could not find any stable phenomenon in the finite condition, and more information will be presented in the next section.

Phase plane portraits of HTL system are shown in Figure 11. If $K_{v,is}c_s > 0$, the stable node is (x^∞, y^∞), so any trajectory will approach (x^∞, y^∞) when $t \longrightarrow \infty$.

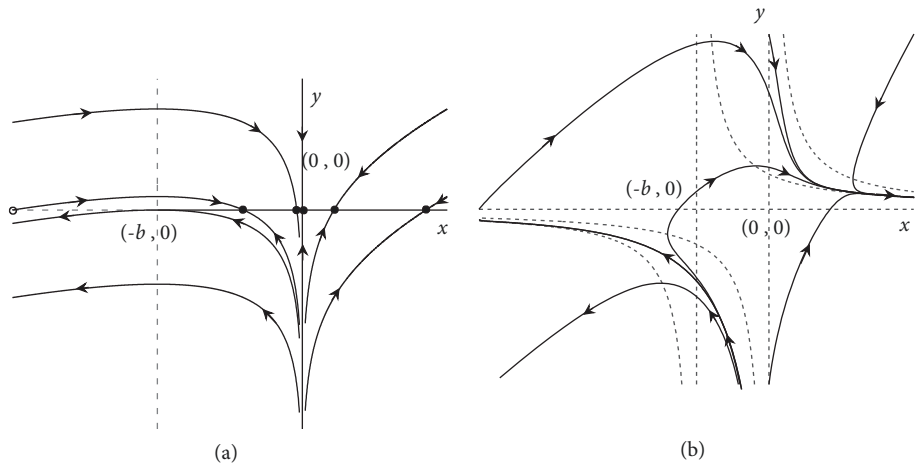

Figure 10: Phase plane portraits of system (2) with $a = 0, b > 0$ and (a) $c = 0$ and (b) $c > 0$.

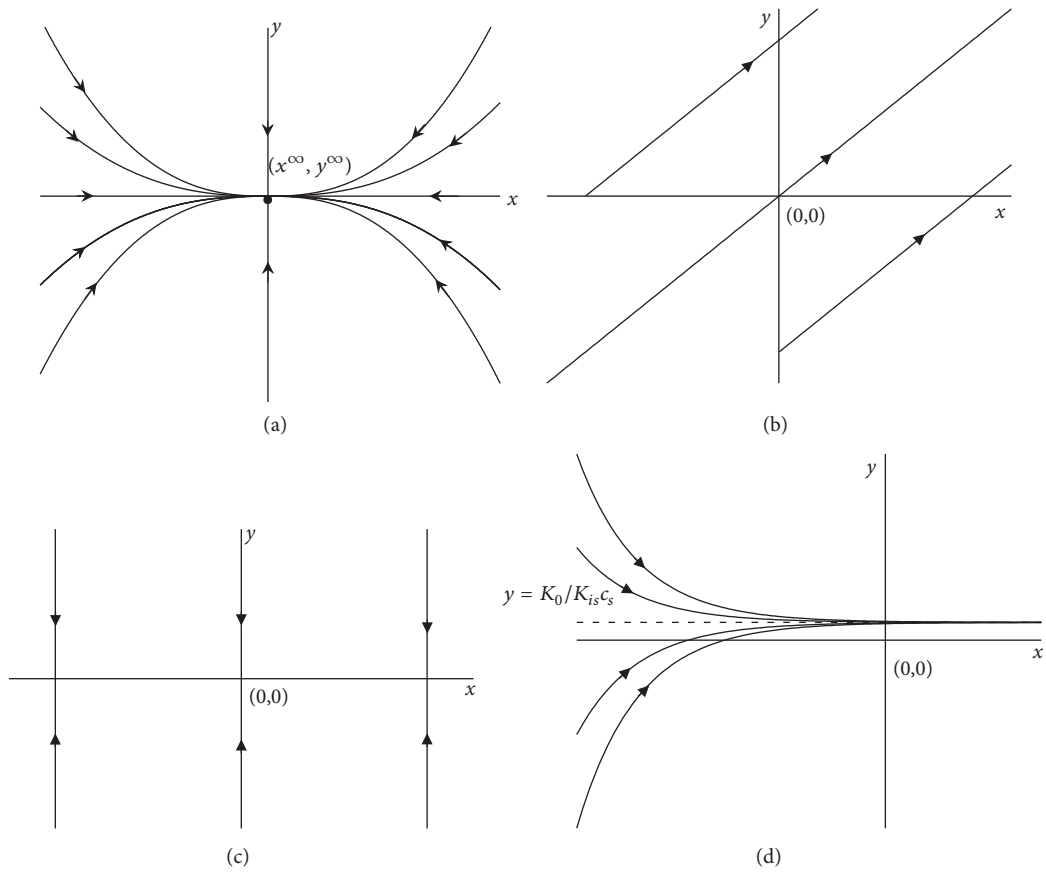

Figure 11: Phase plane portraits of system (1) if $K_{iv} = 0$ and (a) $K_{v,is}c_s > 0$, (b) $K_{v,is}c_s = 0, K_0 > 0$, (c) $K_{vs}c_s = 0, K_{is}c_s > 0, K_0 = 0$, and (d) $K_{vs}c_s = 0, K_{is}c_s > 0, K_0 > 0$.

The global phase portraits for annealing and in-pile processes cannot be easily constructed from the phase plane behaviors of degenerated systems.

3.3. Global Phase Trajectory on Poincaré Disk. Next, we analyze the behaviors at infinity of system (2). First, transform x and y in Poincaré and time

$$\begin{aligned} u &= \frac{y}{x}, \\ z &= \frac{1}{x}, \\ \mathrm{d}t &= z\mathrm{d}\tau \end{aligned} \tag{38}$$

System (2) becomes

$$\begin{aligned} \frac{\mathrm{d}u}{\mathrm{d}\tau} &= z^2 Q\left(\frac{1}{z}, \frac{u}{z}\right) - uz^2 P\left(\frac{1}{z}, \frac{u}{z}\right) \\ &= u(u-1) + (au-b)uz + c(1-u)z^2 \\ \frac{\mathrm{d}z}{\mathrm{d}\tau} &= -z^3 P\left(\frac{1}{z}, \frac{u}{z}\right) = z\left(u + az - cz^2\right) \end{aligned} \tag{39}$$

Let $z = 0$ and the singular points of system (39) are

$$\begin{aligned} &C(0,0) \\ &\text{and } B(1,0) \end{aligned} \tag{40}$$

Theorem 17. *If $a, b > 0$, the singular point of system (39) $C(0,0)$ is a saddle-node. And $B(1,0)$ is an unstable node.*

Proof. At $C(0,0)$, the Jacobi matrix of (39) is

$$\mathbf{J}(0,0) = \begin{pmatrix} -1 & 0 \\ 0 & 0 \end{pmatrix} \tag{41}$$

The trace of (41) is $T = -1 < 0$ and the determinant $J = 0$, so $C(0,0)$ is nonhyperbolic singular point. Similarly, at $B(1.0)$, the trace is $T = 2 > 0$ and the determinant $J = 1 > 0$, so $B(1,0)$ is an unstable node.

For nonhyperbolic singular point $C(0,0)$, system (39) can be written as

$$\begin{aligned} \dot{u} &= u(u-1) + (au-b)uz + c(1-u)z^2 \\ &= -u + \Psi(u,z) \end{aligned} \tag{42a}$$

$$\dot{z} = z\left(u + az - cz^2\right) = \varphi(u,z) \tag{42b}$$

Letting $\dot{u} = 0$, we have

$$u = \left(c + \frac{(b-a)^2}{8}\right) + o\left(z^2\right) \tag{43}$$

Inserting (43) into (42b), we have the expansion

$$\varphi(u,z) = az^2 + \frac{(b-a)^2}{8}z^3 + o\left(z^4\right) \tag{44}$$

So, if

(1) $a \neq 0$, the minimal order of x in φ is $m = 2$ and $C(0,0)$ is a saddle-node;

(2) $a = 0$ and $b \neq 0$, it has $m = 3$ and $C(0,0)$ is an unstable node. □

Transform x and y in Poincaré and time:

$$\begin{aligned} v &= \frac{x}{y}, \\ z &= \frac{1}{y}, \\ \mathrm{d}t &= z\mathrm{d}\tau \end{aligned} \tag{45}$$

System (2) becomes

$$\begin{aligned} \frac{\mathrm{d}v}{\mathrm{d}\tau} &= v(v-1) + (a-bu)uz + c(1-v)z^2 \\ \frac{\mathrm{d}z}{\mathrm{d}\tau} &= z\left(v + bz - cz^2\right) \end{aligned} \tag{46}$$

Theorem 18. *If $a, b > 0$, the singular point of system (46) $D(0,0)$ is a saddle-node.*

Proof. Similarly, we can prove $D(0,0)$ is nonhyperbolic singular point and when

(1) $b \neq 0$, singular point $D(0,0)$ is a saddle-node;

(2) $b = 0$ and $a \neq 0$, singular point $D(0,0)$ is an unstable node.

So, if $a, b > 0$, $D(0,0)$ is a saddle-node. □

For degenerate systems, we could get the following conclusions by the similar process.

Theorem 19. *If $a = b = 0$, the singular point $C(0,0)$ is a nonisolated point and $B(1,0)$ is an unstable node and $D(0,0)$ is a nonisolated point.*

Theorem 20. *If $a = 0, b > 0$, the singular point $B(1,0)$ is an unstable node and $D(0,0)$ is a saddle-node. $C(0,0)$ is a nonisolated point if $c = 0$ and is a saddle-node if $c > 0$.*

The behaviors of global phase portraits on Poincaré disk are similar to the phase plane portraits (Figure 8). As for the infinity, we found that B_1, C_2, and D_2 are unstable nodes. B_2 and (x_1, y_1) are stable node, and C_1, D_1, and (x_2, y_2) are saddle point, as shown in Figure 12.

The global phase portraits of degenerate system on Poincaré disk are shown in Figure 13. For SFL system, the singular points degrade to singular line $xy = c$, such that $C(0,0)$ and $D(0,0)$ change to the nonisolated points. But the behaviors at $B(1,0)$ are unchanged. For LTL system, the behaviors at $C(0,0)$ and $B(1,0)$ are unchanged. But $C(0,0)$ becomes a nonisolated point if $c = 0$, for singular points become singular line $y = 0$. And $C(0,0)$ becomes a saddle-node if $c > 0$ for (x_1, y_1) and (x_1, y_1) shift to $(+\infty, 0)$ and $(-\infty, 0)$, respectively.

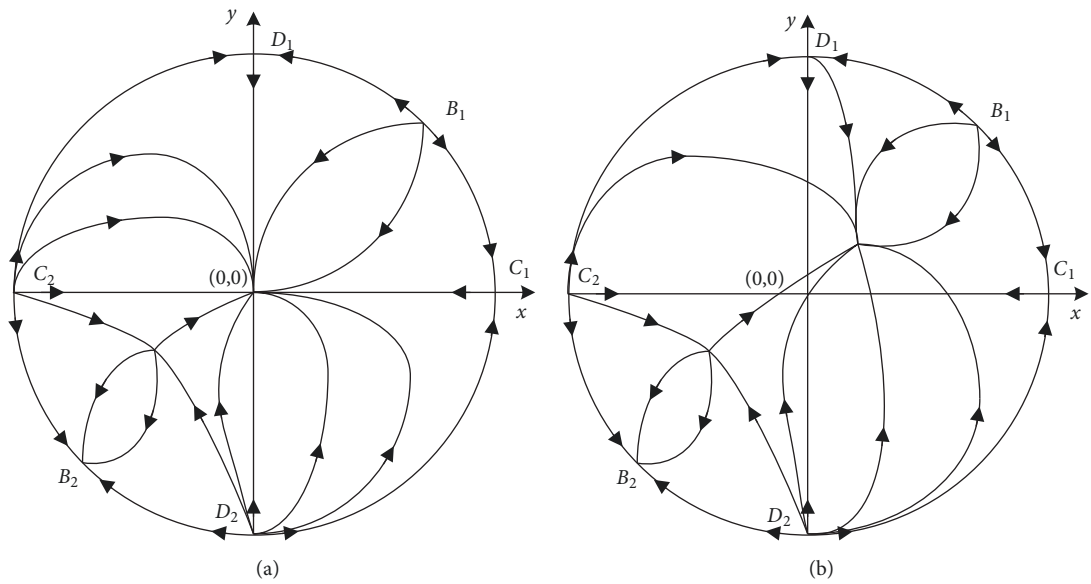

FIGURE 12: Global phase portraits on Poincaré disk of system (2) if (a) $a, b > 0, c = 0$ and (b) $a, b > 0, c > 0$.

4. Admissibility and Numerical Examples

From the definition of vacancy and interstitial, we know that $c_{v,i} = 0$ represents the perfect atom lattice and $c_{v,i} = 1$ means that the lattice is occupied by vacancy or interstitial completely. Thus, for system (2), only if $0 \le x(t), y(t) \le 1$, the concentration could be thought as admissible. So we define the admissible zone

$$\Omega_{ad} = \{(x, y) \mid 0 \le x \le 1, 0 \le y \le 1\} = [0, 1] \times [0, 1] \quad (47)$$

Definition 21. A singular point is admissible if it is inside Ω_{ad}.

Definition 22. A trajectory starting from a point $(x_0, y_0) \in \Omega_{ad}$ is admissible if $(x(t), y(t)) \in \Omega_{ad}$ for any $t > 0$.

Definition 23. A trajectory starting from a point $(x_0, y_0) \in \Omega_{ad}$ is partly admissible if $(x(t), y(t)) \notin \Omega_{ad}$ for sufficiently large t.

4.1. Admissibility of Singular Points and Trajectories. During the annealing process, the stable node $(x_1, y_1) = (0, 0)$ and any trajectory starting from $(x_0, y_0) \in \Omega_{ad}$ are always inside Ω_{ad}. Thus, they are always admissible. However, during the in-pile process, the stable singular point can be shifted outside the admissible zone, and we have the following.

Theorem 24. *(i) The stable node (x_1, y_1) (12) is admissible if and only if*

$$c \le \min\left(b + \frac{b}{a}, a + \frac{a}{b}\right) \quad (48)$$

(ii) The trajectories are partly admissible if and only if

$$\min(a, b) < c \le \min\left(b + \frac{b}{a}, a + \frac{a}{b}\right) \quad (49)$$

(iii) The trajectories are always admissible if and only if

$$c \le \min(a, b) \quad (50)$$

Proof. Letting

$$0 \le x_1 = -\frac{b}{2}\left(1 - \sqrt{1 + \frac{4c}{ab}}\right) \le 1$$
$$0 \le y_1 = -\frac{a}{2}\left(1 - \sqrt{1 + \frac{4c}{ab}}\right) \le 1 \quad (51)$$

we get admissible condition (48) for the stable node.

Assuming $a < b$, only if line $P = 0$ is negative at $x = 1$, the trajectories are admissible; that is,

$$y(x = 1) = \frac{-ax + c}{x} = -a + c \le 0 \quad (52)$$

And (52) can be expand to (50) after adding case $a > b$.

Then, the partly admissible condition (49) is the difference set of (48) and (50). □

As shown in Figure 14(a), if the parameters adopted satisfy the admissible condition (50), any trajectory starting from $(x_0, y_0) \in \Omega_{ad}$ is always inside Ω_{ad} for any $t > 0$. But if the parameters adopted satisfy the partly admissible condition (49), as shown in Figure 14(b), even though every trajectory reaches (x_1, y_1) at last, we could clearly find that some trajectories starting inside Ω_{ad} can go outside during the process.

During annealing process, or if the point production rate is small during in-pile process, the stable node and trajectories are always admissible. If the defect production rate is large, the trajectories are partially admissible or inadmissible. The balance equation is no longer applicable.

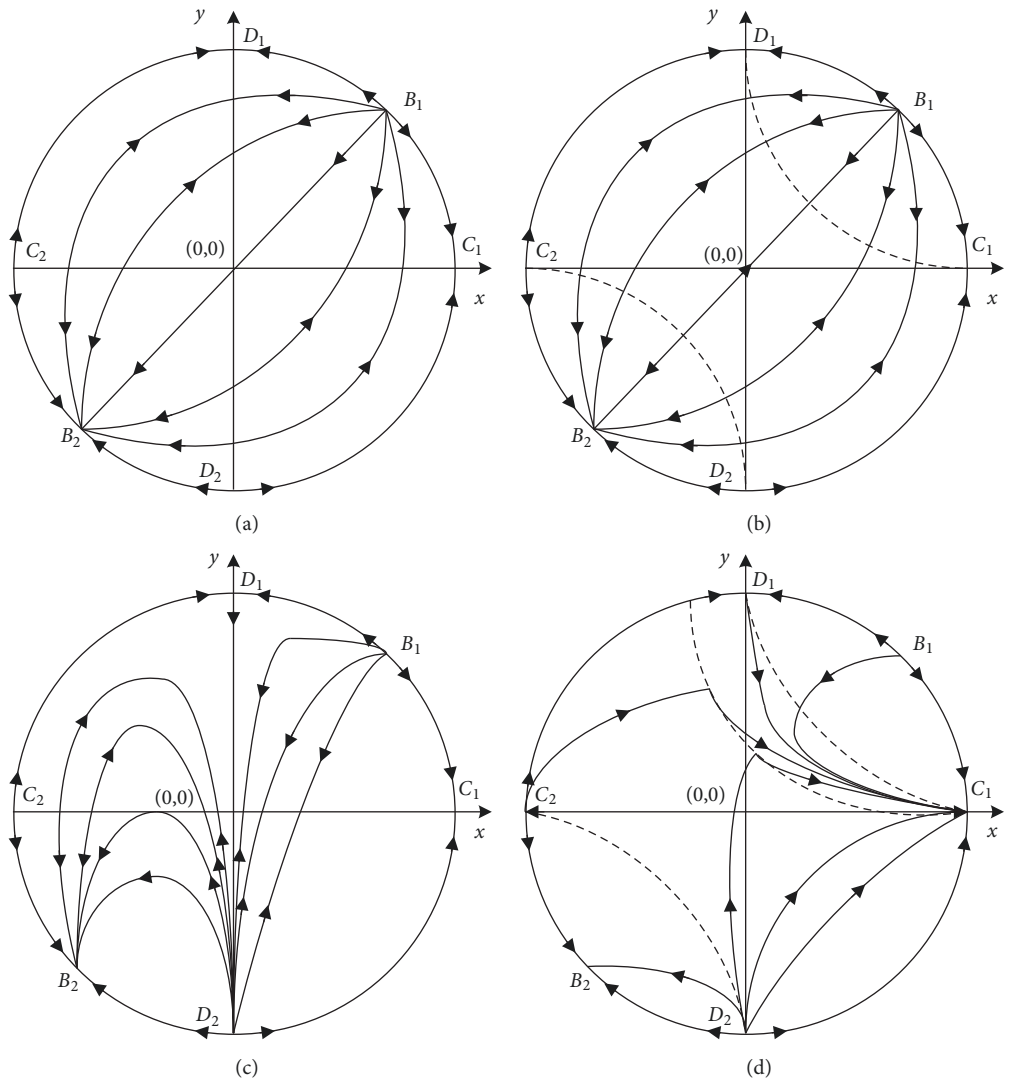

FIGURE 13: Global phase portraits on Poincaré disk of system (2) if (a) $a = b = c = 0$, (b) $a = b = 0, c > 0$, (c) $a = 0, b > 0, c = 0$, and (d) $a = 0, b > 0, c > 0$.

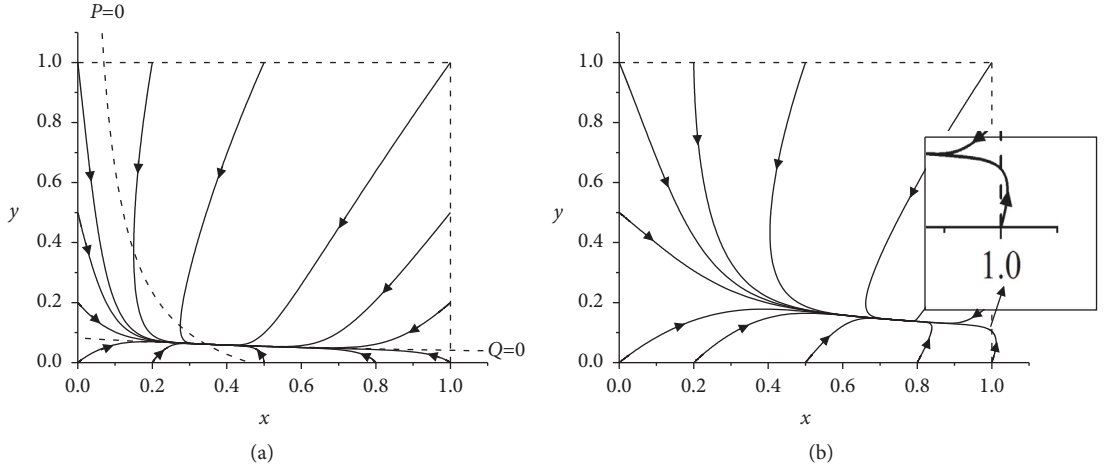

FIGURE 14: (a) Admissible and (b) partly admissible phase plane portraits.

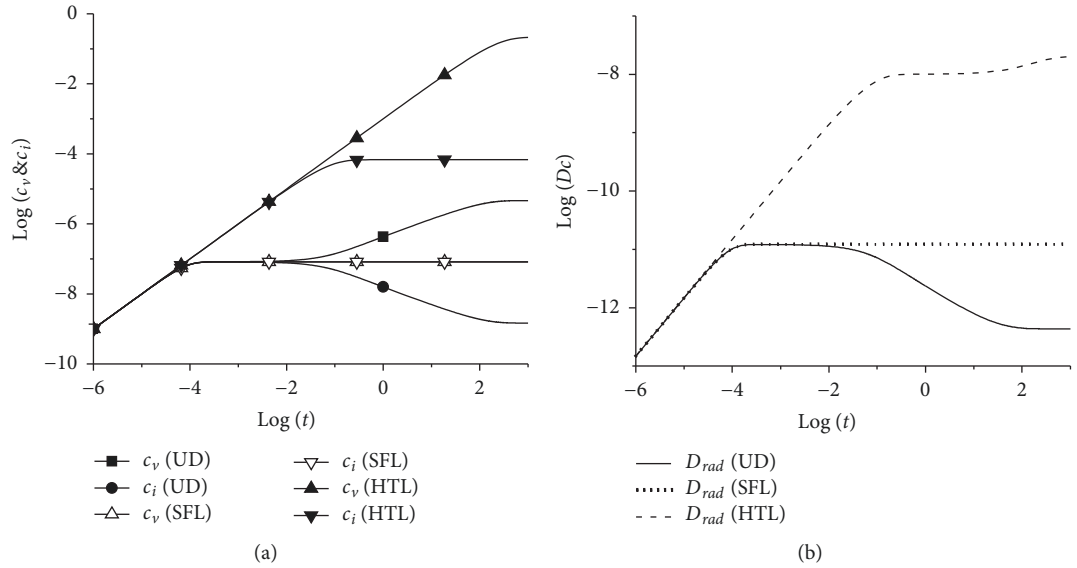

Figure 15: The evolutions of (a) point defects concentration and (b) irradiation enhanced diffusion coefficient of UD, SFL, and HTL system.

Table 1: Calculating parameters for ND, SFL, and HTL system.

	K_{vi} [s^{-1}]	K_{vs} [s^{-1}]	K_{is} [s^{-1}]	c_s	c_v^s	c_i^s
ND	1.47×10^{11}	0.0047	14.7	1×10^5	4.6268×10^{-6}	1.4701×10^{-9}
SFL	1.47×10^{11}	0.0047	14.7	0	0.25×10^{-8}	0.25×10^{-8}
HTL	0	0.0047	14.7	1×10^5	0.2141	6.8×10^{-5}

4.2. Numerical Examples for Defects Evolutions. For better illustration, the evolutions of point defect concentrations and irradiation enhanced diffusion coefficients of UD, SFL, and HTL system during in-pile process will be presented in the following.

The temperature and defects generation rate are taken as $T = 550$K, $K_0 = 1 \times 10^{-3} s^{-1}$. According to the literature [4], the parameters for calculation are shown in Table 1.

In the experiments, the defect concentrations are usually hard to be traced. But it is possible to use the Zener relaxation time [5, 7, 18] to study the diffusion processes during irradiation. Zener relaxation could be also noted as the enhanced diffusion coefficient about [5, 19]

$$D_{rad} = D_v c_v + D_i c_i \tag{53}$$

As shown in Figure 15(a), the evolutions of vacancy and interstitial of UD system are quite different from the degenerate systems. Initially, both concentrations increase linearly following $K_0 t$. Then, the curve has a platform known as quasi-steady state [1], which is exactly the stable state of the SFL system. After that, the vacancy concentration goes on increasing but interstitial decreases. The value of c_v is much larger than c_i at the stable node. The stable concentrations of HTL system are larger than others.

Initially, the concentrations of point defects are too small and result in the small effect of recombination or reaction with sinks. So they increase linearly. With the increase of concentrations, the generation of the point defects is compensated by the recombination, corresponding to the quasi-steady state. After that, the interstitials start to find the sinks and annihilate, and the concentration decreases. At the same time, vacancy concentration goes on increasing for less recombination.

As shown in Figure 15(b), it is easy to find that the evolutions of D_{rad} are similar to the evolutions of interstitial concentration. $D_i c_i$ determines the D_{rad} most of time, but the contributions of vacancy and interstitial are the same at last. The results qualitatively agree to the experimental observations [5].

5. Conclusions

In this paper, the point defect balance equations are analyzed by the qualitative method of ordinary differential equations for the first time. The behaviors of the defects evolution during the annealing and the in-pile processes have been studied. We get the following conclusions:

(1) Two singular points exist for both annealing and in-pile processes. One is a stable node and the other is a saddle point. The stable node is at the origin for annealing such that the steady state is defect free. It is shifted to a defective state when the material is in-pile. Under very large irradiations, the shift can be too much such that the stable node goes outside the physically admissible region. Then, the material becomes amorphous and the PDBE model is no longer physically relevant.

(2) Local behavior near the stable node is affected by the irradiation as well. While the trajectories approach the origin

with the two axes as the stable subspaces for annealing, the stable subspaces are rotated to be nonorthogonal under irradiations. Moreover, even when the stable node and the initial state are both inside the admissible region, it can happen that the trajectory goes outside for a while before entering again.

(3) No closed trajectory can exist and the global behavior is determined by the two singular points and the other six at infinity. The global phase portraits for annealing and inpile processes are qualitatively very similar. But they are very different and cannot be easily constructed from the phase plane behaviors of degenerated systems.

Data Availability

The calculating data used to support the findings of this study are included within the article.

Conflicts of Interest

The authors declare that they have no conflicts of interest.

Acknowledgments

This work was supported by the National Natural Science Foundation of China (nos. 11272092, 11772094, and 11461161008) and the National Science and Technology Major Project of China (nos. 2016YFB0700103, 2017ZX06002006).

References

[1] G. S. Was, *Fundamentals of radiation materials science: metals and alloys*, Springer, New York, NY, USA, 2nd edition, 2016.

[2] L. K. Mansur, "Theory and experimental background on dimensional changes in irradiated alloys," *Journal of Nuclear Materials*, vol. 216, no. C, pp. 97–123, 1994.

[3] S. J. Zinkle and B. N. Singh, "Analysis of displacement damage and defect production under cascade damage conditions," *Journal of Nuclear Materials*, vol. 199, no. 3, pp. 173–191, 1993.

[4] G. J. Dienes and A. C. Damask, "Radiation enhanced diffusion in solids," *Journal of Applied Physics*, vol. 29, no. 12, pp. 1713–1721, 1958.

[5] R. Sizmann, "The effect of radiation upon diffusion in metals," *Journal of Nuclear Materials*, vol. 69-70, no. C, pp. 386–412, 1978.

[6] S. Takaki, J. Fuss, H. Kugler, U. Dedek, and H. Schultz, "The resistivity recovery of high purity and carbon doped iron following low temperature electron irradiation," *Radiation Effects and Defects in Solids*, vol. 79, no. 1-4, pp. 87–122, 1983.

[7] M. Halbwachs, J. Hillairet, and J. R. Cost, "The dynamics of the defect populations associated with electron irradiation in an FCC Ag-Zn alloy," *Journal of Nuclear Materials*, vol. 69-70, no. C, pp. 776–779, 1978.

[8] O. El-Atwani, J. E. Nathaniel, A. C. Leff, K. Hattar, and M. L. Taheri, "Direct observation of sink-dependent defect evolution in nanocrystalline iron under irradiation," *Scientific Reports*, vol. 7, no. 1, 2017.

[9] W. M. Lomer, "Diffusion coefficients in copper under fast neutron irradiation," UKAEA Report AERE-T, 1954.

[10] A. D. Brailsford and R. Bullough, "The rate theory of swelling due to void growth in irradiated metals," *Journal of Nuclear Materials*, vol. 44, no. 2, pp. 121–135, 1972.

[11] P. T. Heald and M. V. Speight, "Point defect behaviour in irradiated materials," *Acta Metallurgica et Materialia*, vol. 23, no. 11, pp. 1389–1399, 1975.

[12] N. M. Ghoniem and G. L. Kulcinski, "A rate theory approach to time dependent microstructural development during irradiation," *Radiation Effects and Defects in Solids*, vol. 39, no. 1, pp. 47–56, 1978.

[13] A. D. Brailsford, R. Bullough, and M. R. Hayns, "Point defect sink strengths and void-swelling," *Journal of Nuclear Materials*, vol. 60, no. 3, pp. 246–256, 1976.

[14] R. W. Balluffi, "Vacancy defect mobilities and binding energies obtained from annealing studies," *Journal of Nuclear Materials*, vol. 69-70, no. C, pp. 240–263, 1978.

[15] C.-C. Fu, J. D. Torre, F. Willaime, J.-L. Bocquet, and A. Barbu, "Multiscale modelling of defect kinetics in irradiated iron," *Nature Materials*, vol. 4, no. 1, pp. 68–74, 2005.

[16] S. Lynch, *Dynamical systems with applications using MapleTM*, Springer Science & Business Media, New York, 2nd edition, 2009.

[17] C. Chicone, *Ordinary differential equations with applications*, Springer Science & Business Media, New York, 2nd edition, 2006.

[18] M. Halbwachs and J. Hillairet, "Identification and dynamic characteristics of the defects responsible for the radiation enhancement of atomic mobility in concentrated α-AgZn alloys," *Physical Review B: Condensed Matter and Materials Physics*, vol. 18, no. 9, pp. 4927–4937, 1978.

[19] A. I. Van Sambeek, R. S. Averback, C. P. Flynn, M. H. Yang, and W. Jäger, "Radiation enhanced diffusion in MgO," *Journal of Applied Physics*, vol. 83, no. 12, pp. 7576–7584, 1998.